Particle size dependent sinterability and magnetic properties of recycled HDDR Nd–Fe–B powders consolidated with spark plasma sintering

Ikram, Awais; Mehmood, Farhan; Sheridan, Richard; Awais, Muhammad; Walton, Allan; Eldosouky, Anas; Sturm, Saso; Kobe, Spomenka; Rozman, Kristina Zuzek

DOI:
10.1016/j.jre.2019.02.010

Journal of Rare Earths 38 (2020) 90–99

Contents lists available at ScienceDirect

Journal of Rare Earths

journal homepage: http://www.journals.elsevier.com/journal-of-rare-earths

Particle size dependent sinterability and magnetic properties of recycled HDDR Nd–Fe–B powders consolidated with spark plasma sintering☆

Awais Ikram [a, b, *], Farhan Mehmood [a, b], Richard Stuart Sheridan [c], Muhammad Awais [c], Allan Walton [c], Anas Eldosouky [b, d], Saso Sturm [a, b], Spomenka Kobe [a, b], Kristina Zuzek Rozman [a, b]

[a] Department for Nanostructured Materials, Jožef Stefan Institute, Jamova 39, SI-1000 Ljubljana, Slovenia
[b] Jožef Stefan International Postgraduate School, Jamova 39, SI-1000 Ljubljana, Slovenia
[c] School of Metallurgy and Materials, University of Birmingham, Edgbaston, Birmingham, B15 2TT, United Kingdom
[d] Magneti Ljubljana, d.d., Stegne 37, SI-1000 Ljubljana, Slovenia

ARTICLE INFO

Article history:
Received 8 November 2018
Received in revised form
12 February 2019
Accepted 15 February 2019
Available online 23 July 2019

Keywords:
Reprocessing end-of life scrap
Rare earth permanent magnets
HDDR
$Nd_2Fe_{14}B$
Recycling
Spark plasma sintering

ABSTRACT

The dependence of the magnetic properties on the particle size of recycled HDDR Nd–Fe–B powders was investigated, with the aim to assess the reprocessing potential of the end-of-life scrap magnets via spark plasma sintering (SPS). The as received recycled HDDR powder has coercivity (H_{ci}) = 830 kA/m and particles in the range from 30 to 700 μm (average 220 μm). After burr milling, the average particle size is reduced to 120 μm and subsequently the H_{ci} of fine (milled) powder was 595 kA/m. Spark plasma sintering was exploited to consolidate the nanograined HDDR powders and limit the abnormal grain coarsening. The optimal SPS-ing of coarse HDDR powder at 750 °C for 1 min produces fully dense magnets with H_{ci} = 950 ± 100 kA/m which further increases to 1200 kA/m via thermal treatment at 750 °C for 15 min. The burr milled fine HDDR powder under similar SPS conditions and after thermal treatment results in H_{ci} = 940 kA/m. The fine powder is further sieved down from 630 to less than 50 μm mesh size, to evaluate the possible reduction in H_{ci} in relation to the particle size. The gain in oxygen content doubles for <50 μm sized particles as compared with coarser fractions (>200 μm). The XRD analysis for fractionated powder indicates an increase in Nd_2O_3 phase peaks in the finer (<100 μm) fractions. Similarly, the H_{ci} reduces from 820 kA/m in the coarse particles (>200 μm) to 460 kA/m in the fine sized particles (<100 μm). SPS was done on each HDDR powder fraction under the optimal conditions to measure the variation in H_{ci} and density. The H_{ci} of SPS-ed coarse fraction (>200 μm) is higher than 930 kA/m and it falls abruptly to just 70 kA/m for the fine sized particles (<100 μm). The thermal treatment further improves the H_{ci} to >1000 kA/m only up to 100 μm sized fractions with >90% sintered density. The full densification (>99%) is observed only in the coarse fractions. The loss of coercivity and lack of sinterability in the fine sized particles (<100 μm) are attributed to a very high oxygen content. This implies that during recycling, if good magnetic properties are to be maintained or even increase the HDDR powder particles can be sized down only up to ≥100 μm.

1. Introduction

The Nd–Fe–B type rare earth permanent magnets since 1984[1,2] have found applications in electric motors, microelectronics, MRI machines and wind turbine generators.[3] The 2011 rare earth crisis has jeopardized the supply chain of rare earth permanent magnets,[4] without any significant success in developing the rare earth free permanent magnets.[3,5,6] Therefore, the researchers are keen to

☆ **Foundation item:** Project supported by European Community's Horizon 2020 Program [H2020/2014-2019] under grant Agreement No. 674973 (MSCA-ETN DEMETER).
* Corresponding author. Department for Nanostructured Materials, Jožef Stefan Institute, Jamova 39, SI-1000 Ljubljana, Slovenia.
E-mail address: rana.awaisikram@yahoo.com (A. Ikram).

https://doi.org/10.1016/j.jre.2019.02.010

recycle the end-of-life permanent magnets and reutilize them directly. Alternatively, the treatments like re-sintering, melt-spinning and hydrogen related processing: hydrogen decrepitation (HD) and the hydrogenation–disproportionation–desorption–recombination (HDDR)[7–20] are possible in direct recycling of the magnetic scrap. The melt spinning and hydrogen routes are more promising from the economical perspective as the powder is directly suited for bonded magnet applications. The nanocrystalline powders cannot be conventionally sintered because of the microstructure dependent magnetic properties i.e., the coercivity will be lost by such processing. The HDDR powder finds most of its commercial applications in isotropic and anisotropic bonded magnets,[14,19] which have relatively lower magnetic properties than the sintered counterparts.

Refining the grain size is a well-established way to enhance the coercivity of Nd–Fe–B type permanent magnets.[21] However, the nanocrystalline Nd–Fe–B powder are highly prone to oxidation due to formation of stable di-hexagonal close packed (dhcp) Nd_2O_3 oxides[22–31] especially with the increase in temperature, thereby restricting the top down operations as well as the recycling process.[9–12,15–20] It was shown that the lower oxygen content and pore free microstructure inhibit the grain coarsening in the sintered magnets,[32] because higher oxygen content means more fcc-Nd to be scavenged out of the grain boundaries, forming hcp and eventually hcp Nd_2O_3. The formation of these oxides causes defects at the intergranular junctions that locally reduce the magnetocrystalline anisotropy of $Nd_2Fe_{14}B$ grains.[27–30] These intergranular defects also introduce strains along the Nd–Fe–B 2:14:1 matrix grain interfaces and act as primary nucleation sites during magnetization reversal.[28]

To preserve the microstructure, the HDDR powder can be sintered by rapid compaction techniques e.g., hot deformation[33,34] or spark plasma sintering (SPS)[35–37] without a significant loss in the magnetic properties. The challenge remains as the HDDR powder is prone to oxidation as Kwon et al.[31] and Takagi et al.[35] reported on the loss of coercivity and remanence due to poorer sinterability in the finer sized HDDR powder, attributing it to the surface oxidation. Preparing the HDDR powder from the as cast ingots allows the freedom to maintain the close particle size range. But the recycling operation becomes tedious on EOL/scrap magnets as they are coated with protective films and the HD treatment cannot be performed without removing the coating. The protective coatings prevent the oxidation of Nd-rich phase in sintered magnets, but the impurities from the secoating will degrade the magnetic properties of the recycled material.[16] Therefore, before the HDDR treatment, the decrepitated powder particles are milled down to <200 μm to sieve out the coating fragments. As the powder particles get smaller (the surface area increases), the Nd-rich phase at the particle boundaries exposed to the surface is prone to oxidation. This limits the applicability as the coercivity drops substantially.[31]

The fundamental aim of this study is to determine the relation between the EOL HDDR-ed Nd–Fe–B particle size to the oxygen content and the SPS sinterability of these recycled HDDR powders. As the hydrogen-based recycling method used to reprocess EOL Nd–Fe–B demands a magnet coating removal, the average particle size of Nd–Fe–B for further reprocessing is reduced below ≤200 μm. To establish the particle size limit for the recycled HDDR-processed powder to be viably reprocessed via SPS we mimicked the real-world conditions of particle size reduction during milling and sieving the fraction to identify the changes in sinterability and the magnetic properties. This research work justifies to what extent the recyclability via SPS as a case example of EOL/scrap magnets and HDDR powder reprocessing is possible. The emphasis of this study is to derive the correlations between the SPS conditions and the particle sizes for obtaining the best magnetic properties out of the recycled HDDR Nd-Fe-B powders.

2. Experimental

Sheridan et al.[13] have provided full details of the HDDR route of producing the recycled powder used in this study. The chemical composition measured with ICP–MS of the recycled powder was $Nd_{13.4}Dy_{0.67}Fe_{78.6}B_{6.19}Nb_{0.43}Al_{0.72}$. For this composition, the theoretical density calculated by multiplying the weight fraction and density of individual elements was approximated to 7.57 ± 0.01 g/cm^3. The end-of-life scrap magnets had oxygen content of 0.266 wt%. The oxygen content increased to 0.476 wt% in the recycled powder after the HDDR reprocessing. The coarse recycled HDDR powder was burr milled for 6 h in argon to reduce the average particle size. Sieving was done in glove box from 1000 to <50 μm mesh size. The magnetic properties of recycled HDDR powder and sieved fractions were measured as a bonded magnet with the Lakeshore VSM (self-demagnetization is not adjusted). An Eltra ON 900 oxygen and nitrogen analyzer was used to measure the variation in oxygen content of the HDDR powder (coarse and fine) and in the powder fractions. The crystal phase identification was performed using the XRD (PANalytical Empyrean diffractometer) using Cu Kα radiation analysis on the different particle size fractions of the recycled HDDR powder. The Curie temperature (T_C) of 305 ± 3 °C and endothermic ternary eutectic temperature of 665 ± 4 °C were determined by Jupiter 449 Simultaneous Thermal Analysis (STA) instrument in the range of 30–900 °C using 20 °C/min heating and cooling rates, under argon environment (99.99% purity and flow rate 50 mL/min).

For SPS sintering, about 3 g of the recycled HDDR powder (coarse and fine) and fractionated powder were added to 10 mm graphite dies. Graphite spacers and punches were placed and the dies were packed in vacuum sheets within the glove box to prevent oxidation during handling. Further 5 kN of uniaxial pressing was applied to squeeze the powder compactly without magnetic alignment. Just before the SPS, the chamber was purged with over pressure of Ar gas and vacuum sheets were removed. The dies were then positioned in the Syntex 3000 (DR. SINTER) SPS furnace with a controlled pressure unit. All the SPS experiments were done under 2 Pa dynamic vacuum and 100 MPa uniaxial pressure was continuously applied. Sintering temperature was varied from 650 to 850 °C, with a heating ramp of 100 °C/min. The holding time at the sintering temperature was kept to 1 min. The SPS temperature was controlled with a calibrated infrared pyrometer. After sintering, the samples were ground with 220 grit size SiC papers to remove the graphite foil. The magnetization and demagnetization behavior was measured on a permeameter (Magnet-Physik Dr. Steingroever). The Archimedean principle density measurements were taken on a DENSITEC density-meter by immersing the samples in silicone oil medium.

The post SPS thermal treatments (PST) were accomplished under a dynamic vacuum of $>10^{-3}$ Pa with a heating rate of 50 °C/min within a horizontal tube furnace. The heat treatment was performed at 750 °C for 1 h. Subsequent density and magnetic measurements were made after the thermal treatment. For the scanning electron microscopy (SEM), the samples were finely ground up to 4000 grit and then polished with 1/4 μm diamond paste on the velvet cloth. The microstructural examination was performed with a field emission scanning electron microscope (JEOL 7600F). Electron energy dispersive X-ray spectroscopy (EDS) analysis was performed at 20 keV with a 20 mm^2 Oxford X-Max detector.

3. Results and discussion

3.1. Characterization of coarse recycled HDDR Nd–Fe–B powder

As obtained recycled HDDR Nd–Fe–B powder particles are in the size range of 30–700 μm. Fig. 1(a) shows the low magnification image of the as received coarse HDDR powder particles with random morphology and an average particle size of 220 μm. Fig. 1(b) shows the typical microstructure of the HDDR powder with the gray matrix phase composed of nanocrystalline $Nd_2Fe_{14}B$ hard magnetic grains (240–400 nm) and the bright Nd-rich phase that is randomly distributed along the grain boundaries. NdO_2 type phase were identified via EDXS (Table 1) as the main Nd-rich phase, except for Nd_2O_3 which appeared slightly greyish and more regular in shape.

3.2. Magnetic properties and characterization of coarse SPS reprocessed HDDR powder

The recycled HDDR powder coercivity H_{ci} = 830 kA/m was measured with the VSM (without self-demagnetization adjustment). The coercivity (H_{ci}) is directly related to the microstructure and composition. The peak H_{ci} was achieved by optimizing the SPS reprocessing at 750–800 °C as shown in Fig. 2(a). Subsequently the thermal treatment at 750 °C for 1 h improved all the magnetic characteristics and the H_{ci} increased from 950 to 1195 kA/m for the sample SPS-ed at 750 °C, without a notable increase in the grain size distribution (≤100 nm). The H_{ci} of as SPS-ed samples at 800–850 °C was higher (>1000 kA/m), which is associated with an appreciably higher diffusivity of liquefied Nd-rich phase and better distribution into the grain boundaries.[38] In this case, the thermal treatment only slightly improved the H_{ci} of as SPS-ed samples ≥ 800 °C, since the adequate redistribution of Nd-rich phase was already achieved during sintering, which means that most probably the strain relaxation must have caused this minor increment in H_{ci} after the thermal treatment. The nominal grain size corresponds to 330 ± 120 nm range for the recycled HDDR powder SPS-ed at 750 °C. The H_{ci} started to decline (1150 kA/m) at SPS temperature of 800 °C and further deteriorated to 1112 kA/m for the sample SPS-ed at 850 °C. This reduction in coercivity is facilitated by the rapid grain coarsening above 820 °C.[35,38]

In contrast, the 650–700 °C samples recovered up to 50% H_{ci} only after the thermal treatments. This is due to inadequate redistribution of liquid phase at this temperature range, which is apparent because of lower sintered density. The thermal treatment above this temperature facilitated substantial diffusional transport of the liquid phase from the particle boundaries towards the intergranular channels, which enhances the H_{ci}.[39,40] Moreover, the thermal treatments are associated with smoothening grain surfaces and strain relaxation from the secondary phases (Nd oxides).[41,42]

The B_r and density increased monotonically with the SPS temperature as shown in Fig. 2(b). The B_r reached 0.82 T for fully dense sample at SPS temperature of 800 °C which increased slightly to 0.83 T (BH_{max} = 118 kJ/m^3) with the thermal treatment at 750 °C. As the magnetic alignment of recycled HDDR powder was not made prior to SPS, the B_r in range of 0.8–0.83 T indicates isotropic nature of reprocessed magnets (J_r/J_S = 0.59). Nonetheless, with SPS reprocessing above 700 °C, the density begins to approach the theoretical value of 7.57 ± 0.01 g/cm^3.

Previous work[38,43] confirmed the thermal treatment facilitated in the redistribution of the Nd-rich phase along the hard phase grain boundaries, smoothening the surface of the grains as well as releasing the interfacial strains from hcp-Nd_2O_3 at intergranular junctions.[35,40–42]

3.3. Characterization, properties and SPS reprocessing fineHDDR Nd–Fe–B powder

In order to understand the limit of sizing down the recycled HDDR particles when they are separated from the protective Ni/ composite coatings, the particle size reduction was performed with burr milling. The average particle size was reduced from 220 to 120 μm as shown in Fig. 3(a) which is in fact in the suitable range for sieving out particles without the flakes of the protective coatings. With this reduction in average particle size, the H_{ci} of the fine recycled HDDR powder was also reduced to 595 kA/m (28.3% reduction). The microstructural features of the fine HDDR powder as in Fig. 3(b) are similar to the coarse HDDR powder as presented in Fig. 1(b), with the exception of increased porosity and microcracks. It seemed obvious that additional pores may have formed due to the loss of Nd-rich phase exposed on the surface during burr milling as the powder particles were trimmed.

Utilizing the aforementioned SPS conditions from 650 to 850 °C for 1 min and 100 MPa uniaxial pressure, the measured H_{ci} was reduced by 64% (350 kA/m) at 750 °C from the fine HDDR powder, whereby the coarse HDDR powder yielded 950 kA/m after SPS-ing. Even at higher temperatures, the H_{ci} of as SPS treated fine HDDR powder did not increase over 500 kA/m as shown in Fig. 4(a). With post SPS thermal treatment the H_{ci} recovered and was greater than the starting coarse as well as the fine HDDR powder. Nonetheless, the H_{ci} dropped after burr milling and after thermal treatment, the fine HDDR powder has ~25% lower H_{ci} than the coarse HDDR powder reprocessed under similar conditions. Fig. 4(b) shows that complete densification was only possible for the samples SPS-ed above 750 °C and successively heat treated. The remanence on the contrary increased with the SPS temperature and the sample

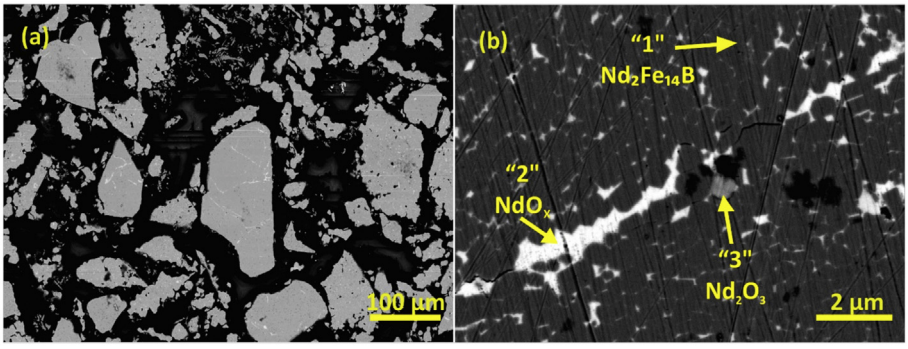

Fig. 1. Backscattered HR-SEM micrographs of the recycled coarse HDDR powder. (a) Particles of average 220 μm size; (b) Intraparticle features showing "1" gray $Nd_2Fe_{14}B$ grains, "2" bright Nd-rich phase in the vicinity of grains and "3" Nd-oxide phase; the pores are black.

Table 1
EDS analysis of recycled HDDR Nd–Fe–B powder.

Phase number	Microstructure feature	Nd [Lα] content (at%)	Fe [Kα] content (at%)	O [Kα] content (at%)	Dy [Lα] content (at%)	Al [Kα] content (at%)
1	$Nd_2Fe_{14}B$	10.6	81.6	4.2	–	1.2
2	NdO_x	24.5	29.5	46.4	–	–
3	Nd_2O_3	27.4	22.1	43.1	0.2	0.3

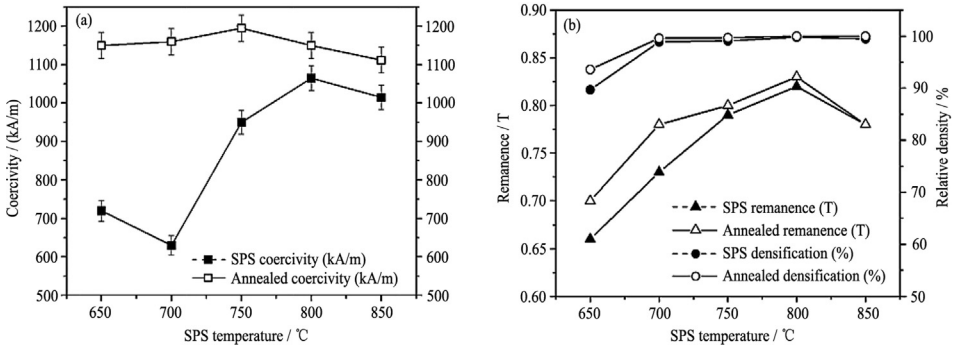

Fig. 2. Effect of SPS temperature and thermal treatment on coercivity H_{ci} (a) and remanence B_r and density (b) of the recycled coarse HDDR powder.

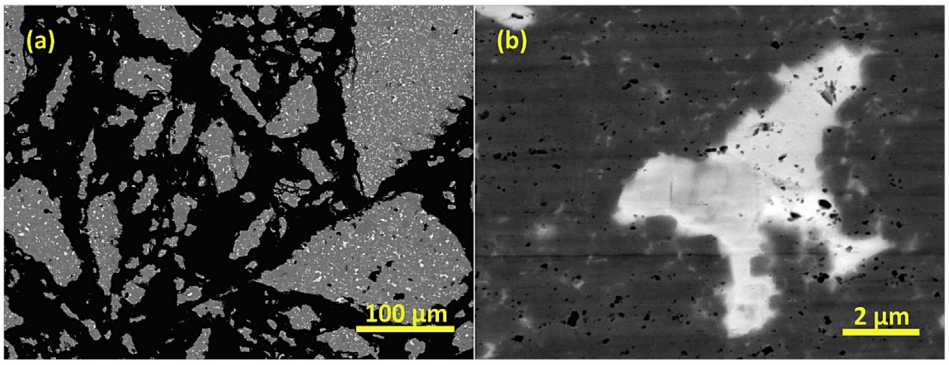

Fig. 3. HR-SEM micrographs of fine HDDR powder of low magnification for particle size distribution (a) and higher magnification image of fine powder grain morphology which is similar to the coarse HDDR powder (b).

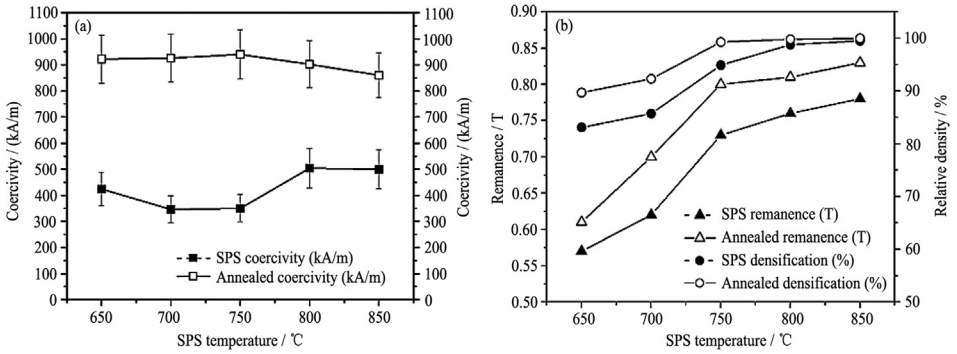

Fig. 4. Magnetic properties of fine HDDR powder after SPS reprocessing and thermal treatment. (a) Coercivity; (b) Density vs remanence.

SPS-ed $\geq$ 750 °C resulted in B_r = 0.8 T (RD. ~98%). The B_r value of 0.83 T (BH_{max} = 116 kJ/m^3) was observed for the 850 °C SPS-ed fine HDDR powder sample after the heat treatment, but the H_{ci} reduced to 880 kA/m. This B_r value was possible at 800 °C in case of the coarse HDDR powder, indicating that fine powders require higher temperature to fully sinter and densify. Since the volume fraction of the $Nd_2Fe_{14}B$ phase is the same after burr milling, and the relative density scales similarly, therefore the deviation in the remanence of the isotropic magnets from coarse and fine powders is negligible as long as experimental relative density reaches 100% of the theoretical value of 7.57 ± 0.01 g/cm^3.

To identify the particle size range suitable for sintering in relation to the oxygen content, the fine HDDR powder was fractioned from 630 μm and down to <50 μm mesh size in the glove box. The effect on magnetic properties by varying the powder particle size after fractionation was studied. The recycled HDDR powders

(coarse and fine) as well as the sieved fractions were analyzed for their nominal oxygen uptake. The oxygen content analysis shown in Fig. 5 revealed that the fine HDDR powder has slightly higher oxygen wt% (5100 ppm) as compared with coarse HDDR powder (4760 ppm), although the average particle size is approximately reduced by 50%. The oxygen content increased rapidly in <100 μm fine sized particles, but the gain is insignificant for particles sized above 200 μm. The oxygen content increased by two folds approx. in <50 μm fraction, even though the milling operation, sieving and oxygen analysis were performed under inert atmosphere. Up to 100 μm, the oxygen content was less than 5500 ppm.

After burr milling, the H_{ci} was reduced by 28% (595 kA/m) in the fine HDDR powder which is obvious due to the gain in oxygen content, as presented in Fig. 6. The H_{ci} measurements were also taken for each sieved fraction. For the coarser fractions (630–200 μm), the measured H_{ci} (830 ± 15 kA/m) was equivalent to the coarse recycled HDDR powder. The 100 μm fraction did not lose much of the coercivity, but the finer sized fractions (<100 μm) experienced a radical coercivity reduction (500 ± 50 kA/m) with higher oxygen uptake. Oxygen scavenges the Nd-rich phase and leads to the formation of Nd_2O_3 phase which considerably reduces the sinterability since the amount of liquid phase for wetting the grains is inadequate and sintered density is much lower.[22–24]

Comparative XRD analysis of coarse, fine and fractionated powders (315, 100, 50 and <50 μm) is given in Fig. 7. The XRD analysis of coarse HDDR powder reveals majority of peaks correspond to hard magnetic $Nd_2Fe_{14}B$ phase with JCPDA serials: 00-036-1296 and 04-006-2691. The lattice parameters of tetragonal $Nd_2Fe_{14}B$ belong to $P42/mnm$ space group with $a = 0.879$ nm, $b = 0.879$ nm and $c = 1.22$ nm. The matrix phase remained the same even after the burr milling and no dissociation to α-Fe was detected. The tetragonal $NdFe_4B_4$ (JCPDA # 01-081-3530) boride phase was also present. Several types of Nd-rich phases were identified with the XRD. The volume fraction of metallic Nd was below the detection limit, hence most of the Nd-rich ensembles comprised of NdO (JCPDA # 04-007-3961) and NdO_2 phases (JCPDA # 04-007-0500). This NdO_x type Nd-rich phases are present in all the samples, irrespective of particle size. The NdO phase peak is observed in all the samples, while NdO_2 peak is more distinguished in 315 and 100 μm fractions as well as the coarse HDDR powder. The NdO_2 peak intensity diminishes in the fine fractions (50 and <50 μm) as well as the milled HDDR powder. With an increasing oxygen content in the smaller particles, the NdO_x phase partially transforms to cubic c-Nd_2O_3 oxide (JCPDA # 00-040-1283). The peaks and relative intensities of c-Nd_2O_3 increased in the fine HDDR powder as well as <100 μm sized fractions. Additionally, the fine HDDR powder and

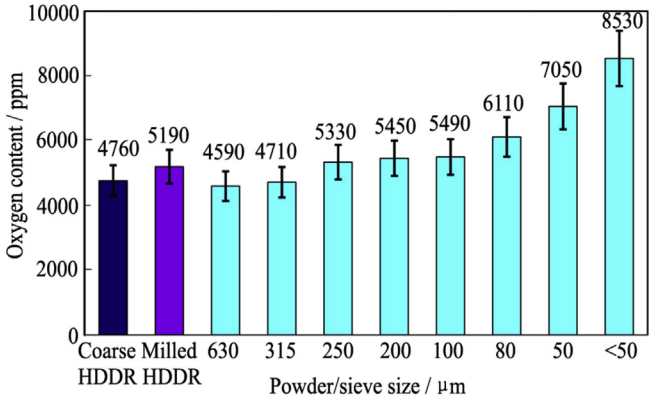

Fig. 5. O_2 content analysis of the coarse, fine and post milling fractionated HDDR powder.

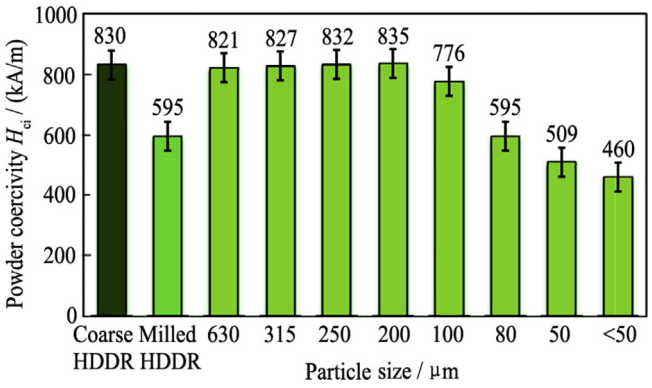

Fig. 6. Coercivity variation with the powder particle size after burr milling.

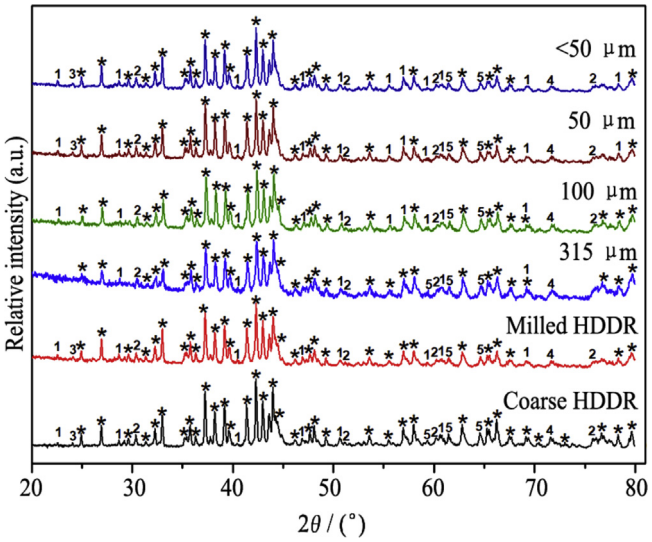

Fig. 7. XRD analysis of coarse, fine and fractions (315, 100, 50 and <50 μm) of recycled HDDR powder. * – tetragonal $Nd_2Fe_{14}B$; 1 – cubic Nd_2O_3; 2 – cubic NdO_2; 3 – hexagonal Nd_2O_3; 4 – tetragonal $NdFe_4B_4$; 5 – cubic NdO.

<100 μm sized fractions also featured hexagonal hcp-Nd_2O_3 type oxide phase (JCPDA # 00-040-1282 and 04-006-0997). This hcp oxide phase is known to introduce larger interfacial strains along the grain boundaries which reduces the H_{ci}.[29,30] With an increasing volume fraction of hcp/cubic Nd_2O_3, the overall grain boundary area is reduced and so the grains experience localized exchange effects without a continuous intergranular phase.[35,37,40] With the increase in oxygen content in finer fractions, the peak intensities of Nd_2O_3 oxides was found to increase, which must be the reason behind the inferior sintered density for the samples SPS-ed up to 750 °C, as in Fig. 4(b). The thermal treatment slightly improved the sintered density, and conversely higher SPS temperatures (≥800 °C) was required to fully densify the fine HDDR powder.

3.4. SPS reprocessing of fractionated fine HDDR powder

These powder fractions were SPS reprocessed at 750 and 800 °C to identify how the magnetic properties change for each fraction and knowing the state of oxygen uptake. As shown in Fig. 8(a) and (c), the coarse fractions reproduced $H_{ci} = 900 \pm 50$ kA/m, which is equivalent to the non-milled HDDR powder. The SPS-ed H_{ci} declined below 450 kA/m for ≤200 μm sized fraction in the 750 and

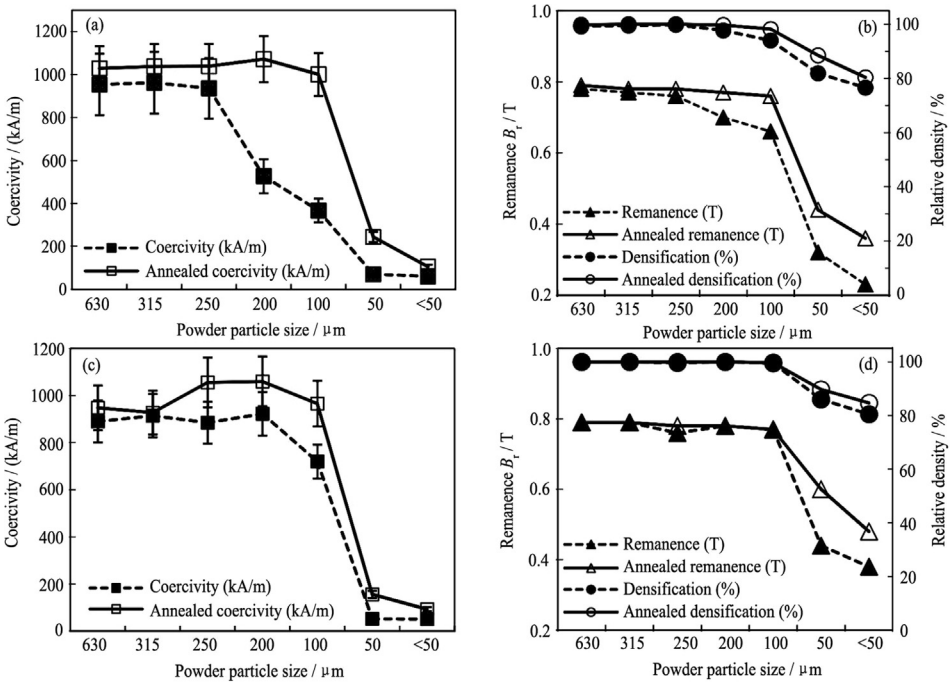

Fig. 8. Magnetic properties of fractionated powder SPS reprocessed at 750 °C (a, b) and at 800 °C (c, d). Dashed lines show magnetic properties after SPS sintering, whereby the properties after the thermally treatment are represented by solid lines.

800 °C SPS-ed samples are shown in Fig. 8(a) and (c), respectively. In the ≤100 μm powder fractions, the H_{ci} got reduced drastically to less than 100 kA/m. The thermal treatment improved the overall H_{ci} in ≥100 μm sized fractions by mere 50–100 kA/m, but nonetheless the H_{ci} was significantly lower than 200 kA/m in the finer sized HDDR powder fractions. The H_{ci} of ≤50 μm fractions after SPS was less than 100 kA/m and only increased to −245 kA/m, which is substantially lower than both the fine HDDR powder (595 kA/m) and <50 μm powder fraction's coercivity (460 kA/m). This is possibly due to a phase transformation during the SPS that further deteriorated the H_{ci} of <100 μm sized fractions. The possible phase transformation during the SPS should be of Nd-rich phase, i.e., of NdO_x and c-Nd_2O_3 to hcp-Nd_2O_3[26–30] for oxygen content greater than 6000 ppm. This also degraded the sinterability as the SPS-ed density of fine fractions was 6.3 and 6.5 g/cm^3 at 750 and 800 °C, respectively.

At SPS reprocessing temperature of 800 °C (Fig. 8(d)) the densification was marginally higher than with the SPS temperature of 750 °C (Fig. 8(b)). The densification dropped as the particle size was reduced below 100 μm. The densification was lower than −80% after the SPS for these fine fractions and after the thermal treatment only improved to approx 84%. Predictably the B_r was approx. 50% lower for the finer fractions (<100 μm) as shown in Fig. 8(b) for 750 °C and (d) for 800 °C SPS-ed fractions. The B_r of the coarse fractions 630 and 315 μm was 0.79 T in 800 °C SPS-ed sample. The coarse fractions sintered at 750 °C had slightly lower remanence (2%) and reached $B_r = 0.79$ T (BH_{max} −108 kJ/m^3) after the thermal treatment. The B_r and density were slightly higher when the powder fractions were SPS-ed at 800 °C, except for the finer fractions (≤100 μm), which did not recover their magnetic properties after the thermal treatment (and not even comparable to the fine HDDR powder). Since the remanence ratio (J_r/J_S −0.58) for the fully dense samples (i.e., coarser fractions (≥100 μm)) does not change substantially with the SPS reprocessing temperatures, the absolute B_r values indicate the miniscule changes in sintered density of the isotropic magnets. The J_r/J_S ratio of 0.34 is significantly lower for the <50 um fraction, implying poor densification of isotropic magnets from the fine HDDR powder.

On the contrary, milling has introduced more oxygen in to the system as the particle size was reduced. The excess of non-oxidized intergranular Nd-rich phase is attributed to improvement in the H_{Ci} of the original HDDR powder[13,40,44] as well as SPS processed magnets.[35–37] So, the presence of pristine NdO_x type enrichments contributed to retaining the H_{ci} after milling and subsequent SPS reprocessing in coarser fractions (≥200 μm). The reduction of 100–200 kA/m H_{ci} in coarse fractions as compared to the non-milled HDDR powder (−1200 kA/m) is due to the mechanical degradation of the powder surfaces which activates the surface for oxygen uptake,[38,43–47] and thermal processing (SPS) permits phase transformation of Nd-oxides, as more of the surface oxygen reacts with intergranular Nd-rich phase to form cubic and hcp-Nd_2O_3.[25–31]

The most obvious reason identified for the degradation of sinterability and the magnetic properties is clearly the exponential gain in the oxygen content, which leads to the formation of hcp-Nd_2O_3 oxide phase. This phase remains stable during the SPS process, and in finer fractions with higher surface area, its occurrence of hcp-Nd_2O_3 phase is more apparent. Therefore, the amount of the liquid phase during SPS is not enough to fully densify the recycled HDDR powder. The lack of formation of optimal microstructure after SPS in finer fractions therefore is the reason why H_{ci}, B_r and the density are low, which do not recover even after the thermal treatment due to substantial oxidation (Nd-rich phase transformation to cubic- and hcp-Nd_2O_3).

The original EOL sintered magnet had H_{Ci} −1160 kA/m, and recycled HDDR powder's coercivity is 830 kA/m. During the HDDR based recycling it is essential that all disproportionated phases especially α-Fe must recombine back to $Nd_2Fe_{14}B$ matrix phase and the Nd-rich intergranular phase is uniformly distributed along the grains. During desorption, the hydrogen dissociates from NdH_2 and promotes the diffusion of Nd during recombination stage by forming continuous grain boundary phase surrounding the

$Nd_2Fe_{14}B$ matrix, which in turn reduces grain's surface defects and increases the H_{Ci}.[48] Such recycled HDDR powder will have magnetic properties close to EOL magnet because of nanostructurization of the $Nd_2Fe_{14}B$ grains i.e., near the single domain grain size.[3,5,13] During the recycling with HDDR process, if Nd content is low or gets reduced as the oxygen scavenges it to form Nd_2O_3, then its uniform distribution will be affected which can cause grain boundary regions running dry. Therefore, the adjacent grains across such dry grain boundary channels are in contact with each other, leading to localized exchange coupling which reduces the coercivity. [3,40] The presence of micron sized residual grains after d-HDDR process can also reduce the HDDR powder coercivity, so control of the HDDR technology and improvements are necessary. [43–47] Excessive addition of Nd and up to 2 at% Al in the composition has been reported to increase the coercivity of HDDR powder to 1560 kA/m due to continuous grain boundary layer of Nd-rich phase,[48] but such methodology may not be applicable to modify the composition of magnetic scrap during the HDDR recycling route. The diffusion treatment of the HDDR powder with up to 20 wt% $Nd_{80}Cu_{20}$ resulted in H_{ci} of 1552 kA/m,[49] may seem a more feasible approach after HDDR recycling to augment the coercivity. However, the target of this study was also to determine the highest possible magnetic properties from the SPS processed recycled HDDR powder, without any addition of RE-rich diffusing alloys.

Comparing the findings of this study with state-of-the-art on recycling and HDDR Nd–Fe–B, it is clear that the obtained $H_{ci} = 1200$ kA/m of coarse non-milled powder is the highest for this composition of the recycled HDDR powder,[13–19, 36–38, 50,51] even compared to our previous results[38] due to application of higher pressure and preservation of the original HDDR microstructure after SPS and optimal thermal treatments. The recovery of H_{ci} values of original EOL magnet asserts that the HDDR recycling route is a very feasible option in terms of retaining the ultrafine microstructure and the correlated magnetic properties. The SPS has proven as an indispensable tool to sinter bulk magnets out of the recycled HDDR powder without compromising on the magnetic properties. The H_{ci} values in this study are slightly higher than the commercial HDDR powder as well,[35] where the authors also described finer particles exhibiting lower magnetic properties but not classifying with an explanation of how oxidation disrupts the microstructure and the effects of annealing in recovery of the magnetic properties.

The initial magnetic properties in the recycled Nd–Fe–B system can be recovered only if the Nd-rich phase remain unattached and/or in NdO_x form which has not been further oxidized to stable hcp-Nd_2O_3 phase, which put a limit on sizing down the particle size to $\geq$100 μm.[38,50] At sintering temperatures used in the present study, it is expected for the oxygen adsorbed on the surface of Nd-rich phase to undergo further oxidation to metastable hcp-Nd_2O_3 phase which consumes more Nd, henceforth the smaller HDDR particles are more prone to this phase transformation[31] during the SPS and thermal treatment. This effectively limits both: the sinterability and the coercivity. When the metallic Nd from the intergranular regions excessively transforms to oxides because of the adsorbed surface oxygen, the diffusion kinetics of Nd-rich liquid phase during the thermal treatment will be limited to redistribute it uniformly across the intergranular region leading to lower coercivities, which would otherwise recover the magnetic properties of the recycled feedstock. The thermal treatment was found to be beneficial as it relieves the microstructure of SPS processing stresses, refines the surface morphology of the matrix grains[3] and the grain boundary channels are widened[40,41,48,49] with the Nd-rich phase being redistributed, which in turn increases the coercivity.

3.5. SEM examination of SPS reprocessed fractions

The SEM analysis in Fig. 9 revealed the coarser fractions (630 and 315 μm) after SPS-ing at 750 °C and subsequently thermally treated, formed up nearly dense microstructure. The Nd-rich phase is adequately distributed along the particle boundaries in the microstructure as shown in Fig. 9(a) and (c) as well as the grain boundary region along of the $Nd_2Fe_{14}B$ matrix phase (b) and (d). The average grain size does not change and it says in the range of

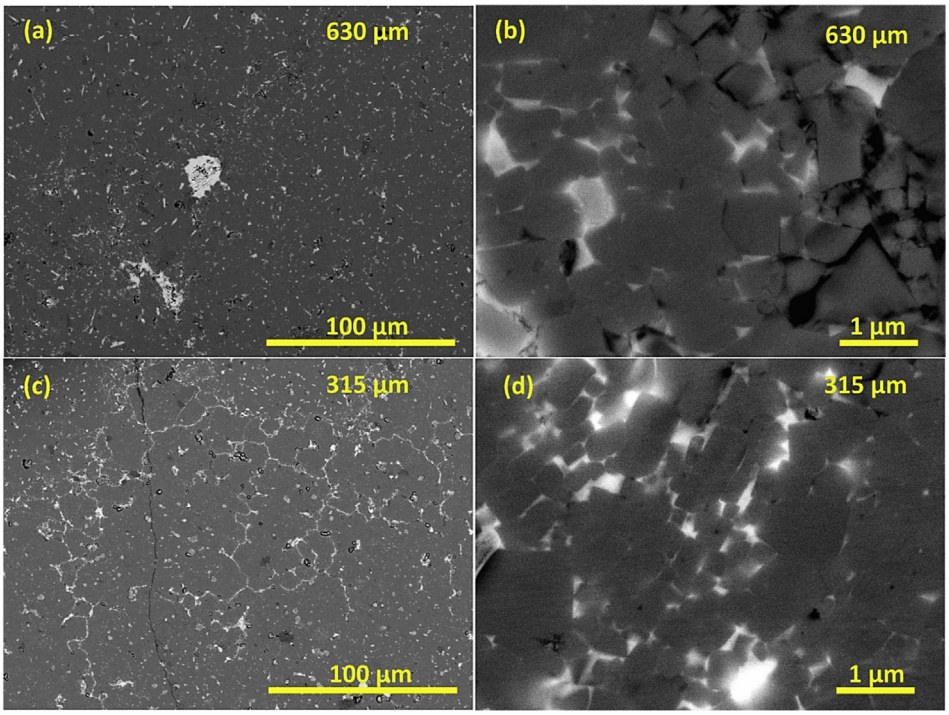

Fig. 9. HR-SEM images of 750 °C SPS treated coarse powder fractions.

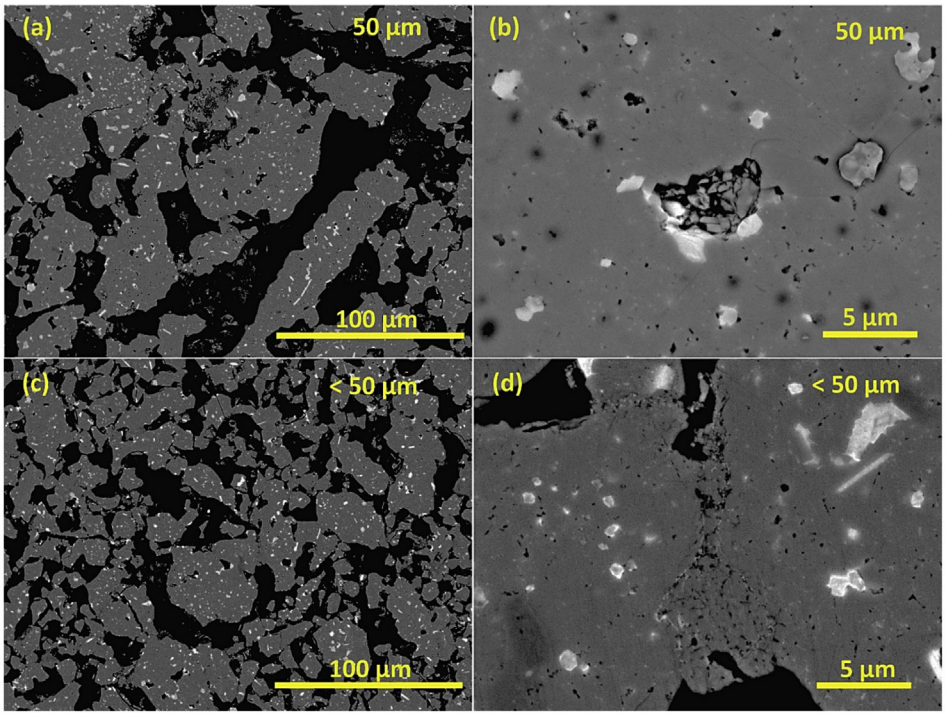

Fig. 10. BSE SEM micrographs of SPS reprocessed finer fractions 50 and <50 μm at 750 °C.

300–500 nm after the burr milling as in Fig. 9(b) of 630 μm and (d) of 315 μm.

Comparatively, the microstructure of the finer sized fractions SPS-ed at 750 °C and thermally treated samples is noticeably different as shown in Fig. 10(a) and (c) of 50 and <50 μm, respectively. Clearly with the reduction in the particle size, overall very high porosity in the microstructure is evident which is attributed to poor sintered densities. The Nd-rich phase is distributed like an extensive network in the coarser fractions (630 and 315 μm) in Fig. 9(a, c), which is contrary to the fine fractions (50 and <50 μm) as the intergranular phase is truncated to the rounded shape. At higher magnification Fig. 10(b) and (d), it was confirmed that these rounded features are Nd_2O_3 type oxides. So in the fine fractions, most of the Nd-rich phase existed with a different (greyish) contrast and morphology which was due to the oxidation of the secondary phase (Nd_2O_3 phase transformation). The intergranular Nd-rich phase was mostly squeezed out to the surface during the SPS and it oxidized on the surface with adsorbed oxygen, subsequently forming Nd_2O_3 as confirmed with EDS, therefore the porosity was left over in these finer fractions. Lower density samples from fine sized HDDR powder had reportedly poorer magnetic properties, which were unrecoverable even after thermal treatments.[35]

This verifies the fact that the overall reduction in the total volume fraction of the hard-magnetic phase after burr milling is virtually insignificant. But the secondary Nd-rich phase experiences phase change due to excessive formation of Nd_2O_3 oxides, which radically drops the recycled powder and sintered magnets' coercivity, moreover reduces the sinterability for finer fractions as well.[22,23,31,40] In effect, it reduces the diffusivity of liquid phase due to excessive Nd_2O_3 oxides formation, therefore loss of Nd-rich liquid phase due to the formation of stable hcp-Nd_2O_3 as the most probable reason for lower sintered density and remanence.[26,28] Even though the interfacial strains associated with Nd_2O_3 formation along intergranular junctions are reduced by thermal treatments which improves overall the magnetic properties as well as the sintered density, it is a fair indicator that a much higher volume fraction of Nd-oxides will ultimately deteriorate the magnetic properties (beyond repair and may require excessive addition of Nd).[25,35,40] Henceforth the presence of secondary phase is very important for the development of optimal magnetic properties and it degrades severely as Nd-rich phases gets exponentially oxidized with the particle size reduction. Thereby it is suggested to maintain the powder particle size >100 μm during the HDDR reprocessing of end-of-life scrap magnets to achieve higher H_{ci} and sintered densities. Alternative recycling strategy should be adopted for coated magnets to remove the protective coatings prior to pulverization of EOL scrap magnet's particles, which must not be below 100 μm if HDDR reprocessing is opted. Moreover, the <100 μm sized recycled HDDR powder may require supplementary RE-rich alloy to recover the degradation of the magnetic properties and sinterability.

4. Conclusions

The magnetic properties and the sinterability of the recycled HDDR Nd–Fe–B powder from end-of-life scrap magnets were evaluated in relation to the oxygen content. Spark plasma sintering was used to fully densify non-milled HDDR powder with H_{ci} values corresponding to fresh commercial grade Aichi Steel's HDDR powder. The fine HDDR powder (<100 μm) underperformed with SPS reprocessing and could not gain similar properties as the coarse HDDR powder (≥100 μm). After the optimal SPS reprocessing at 750 °C for 1 min, the H_{ci} is 945 kA/m of the isotropic sintered magnets made from burr milled recycled powder and the coarser fractions is ~50% higher than this fine HDDR powder. The optimally SPS treated coarser fractions (≥200 μm) have virtually unchanged coercivity (>1000 kA/m) and full densification, similar to the coarse recycled HDDR powder. The finer sieved fractions (≤50 μm) were

found as the culprit behind the radical coercivity drop due to the substantial gain in the oxygen content (>8000 ppm).SEM/EDS analysis confirms the loss of intergranular Nd-rich phase and sweeping formation of Nd_2O_3 phases on the surface of the fine fractionated HDDR powder. Thereby the fine powder size fractions ($\leq$50 μm) loose the sinterability in the SPS and the resultant magnetic properties are poor. Based on our study results the 100 μm particle size is proposed as the minimum limit for reprocessing of the HDDR powder without sacrificing the magnetic properties.

Acknowledgments

The research leading to these results has received the funding from the European Community's Horizon 2020 Program ([H2020/2014-2019]) under Grant Agreement no. 674973 (MSCA-ETN DEMETER). Project website: http://etn-demetereu/. This publication reflects only the authors' views, which are targeted to contribute to the betterment of the global community. The authors duly acknowledge the Department for Nanostructured Materials (K7 Nano) for provisioning the magnet synthesis/measurement facilities and the Center for Electron Microscopy & Microanalysis (CEMM) for scanning electron microscopy analysis at the Jozef Stefan Institute, Slovenia. We also extend our thanks to Mr. Luka Kelhar (MSc.) and Dr. Marjeta Maček Kržmancfor helping with the XRD and DSC measurements respectively, at Jozef Stefan Institute, Slovenia.

References

1. Sagawa M, Fujimura S, Togawa N, Yamamoto H, Matsuura Y. New material for permanent magnets on a base of Nd and Fe (invited). *J Appl Phys*. 1984;55(6):2083.
2. Croat JJ, Herbst JF, Lee RW, Pinkerton FE. Pr-Fe and Nd-Fe-based materials: a new class of high-performance permanent magnets (invited). *J Appl Phys*. 1984;55(6):2078.
3. Sugimoto S. Current status and recent topics of rare-earth permanent magnets. *J Phys D Appl Phys*. 2011;44(6):064001.
4. Binnemans K, Jones PT. Rare earths and the balance problem. *J Sustain Metall*. 2015;1(1):29.
5. Poudyal N, Ping Liu J. Advances in nanostructured permanent magnets research. *J Phys D Appl Phys*. 2013;46(4):043001.
6. Gutfl O, Willard MA, Brück E, Chen CH. *Magnetic Materials and Devices for the 21st Century: Stronger, Lighter, and More Energy Efficient*. 2011:821.
7. Walton A, Yi H, Rowson NA, Speight JD, Mann VSJ, Sheridan RS. The use of hydrogen to separate and recycle neodymium-iron-boron-type magnets from electronic waste. *J Clean Prod*. 2015;104:236.
8. Sheridan RS, Sillitoe R, Zakotnik M, Harris IR, Williams AJ. Anisotropic powder from sintered NdFeB magnets by the HDDR processing route. *J Magn Magn Mater*. 2012;324(1):63.
9. Zakotnik M, Tudor CO. Commercial-scale recycling of NdFeB-type magnets with grain boundary modification yields products with “designer properties” that exceed those of starting materials. *Waste Manag*. 2015;44:48.
10. Kim AS, Kim DH, Namkung S, Janget TS, Lee DH, Kwon HW, et al. Development of high coercive powder from the Nd-Fe-B sintered magnet scrap. *IEEE Trans Magn*. 2004;40(4):2877.
11. Itoh M, Masuda M, Suzuki S, Machida K. Recycling of rare earth sintered magnets as isotropic bonded magnets by melt-spinning. *J Alloys Compd*. 2004;374(1–2):393.
12. Sepehri-Amin H, Ohkubo T, Zaktonik M, Prosperi D, Afiung P, Tudor CO, et al. Microstructure and magnetic properties of grain boundary modified recycled Nd-Fe-B sintered magnets. *J Alloys Compd*. 2017;694:175.
13. Sheridan RS, Williams AJ, Harris IR, Walton A. Improved HDDR processing route for production of anisotropic powder from sintered NdFeB type magnets. *J Magn Magn Mater*. 2014;350:114.
14. Kimiabeigi M, Sheridan RS, Widmer JD, Walton A, Farr M, Schole B, et al. Production and application of HPMS recycled bonded permanent magnets for a traction motor application. *IEEE Trans Ind Electron*. 2018;65(5):3795.
15. Burkhardt C, Weber O, Podmiljsak B, Gonzalez-Gutierrez J, Kukla C, Degri M, et al. Isotropic NdFeB hard magnets: MIM production using recycled powders with and without Nd additions. *Powder Inject Mould Int*. 2017;11(4):75.
16. Li XT, Yue M, Zakotnik M, Liu WQ, Zhang DT, Zuo TY. Regeneration of waste sintered Nd-Fe-B magnets to fabricate anisotropic bonded magnets. *J Rare Earths*. 2015;33(7):736.
17. Li C, Liu WQ, Yue M, Liu YQ, Zhang DT, Zuo TY. Waste Nd-Fe-B sintered magnet recycling by doping with rare earth rich alloys. *IEEE Trans Magn*. 2014;50(12):3.
18. Périgo EA, da Silva SC, Martin RV, Takiishi H, Landgraf FJG. Properties of hydrogenation-disproportionation-desorption-recombination NdFeB powders prepared from recycled sintered magnets. *J Appl Phys*. 2012;111(7):07A725.
19. Gutfleisch O, Güth K, Woodcock TG, Schultz L. Recycling used Nd-Fe-B sintered magnets via a hydrogen-based route to produce anisotropic, resin bonded magnets. *Adv Energy Mater*. 2013;3(2):151.
20. Zakotnik M, Harris IR, Williams AJ. Multiple recycling of NdFeB-type sintered magnets. *J Alloys Compd*. 2009;469(1–2):314.
21. Hono K, Sepehri-Amin H. Strategy for high-coercivity Nd-Fe-B magnets. *Scr Mater*. 2012;67(6):530.
22. Nothnagel P, Müller KH, Eckert D, Handstein A. The influence of particle size on the coercivity of sintered NdFeB magnets. *J Magn Magn Mater*. 1991;101(1–3):379.
23. Li WF, Ohkubo T, Hono K, Sagawa M. The origin of coercivity decrease in fine grained Nd-Fe-B sintered magnets. *J Magn Magn Mater*. 2009;321(8):1100.
24. Liu GZ, Yao HF, Xia N, Zhao MJ, Li B, Yu XJ. Time-stability of sintered Nd-Fe-B permanent magnet with lower oxygen content. *J Rare Earths*. 2010;28(suppl 1):396.
25. Matsuura M, Goto R, Tezuka N, Sugimoto S. Influence of Nd oxide phase on the coercivity of Nd-Fe-B thin films. *Mater Trans*. 2010;51(10):1901.
26. Matsuura M, Fukada T, Goto R, Tezuka N, Sugimoto S. Influences of oxidation state of Nd-rich phaseon the coercivity of Nd-Fe-B/Nd thin films. *Mater Trans*. 2009;50(9):2139.
27. Mo W, Zhang L, Liu Q, Shan A, Wu J, Komuro M. Dependence of the crystal structure of the Nd-rich phase on oxygen content in an Nd–Fe–B sintered magnet. *Scr Mater*. 2008;59(2):179.
28. Hrkac G, Woodcock TG, Butler KT, Saharan L, Bryan MT, Schrefl T, et al. Impact of different Nd-rich crystal-phases on the coercivity of Nd-Fe-B grain ensembles. *Scr Mater*. 2014;70(1):35.
29. Kim TH, Lee SR, Namkumg S, Jang TS. A study on the Nd-rich phase evolution in the Nd-Fe-B sintered magnet and its mechanism during post-sintering annealing. *J Alloys Compd*. 2012;537:261.
30. Kim TH, Lee SR, Lee MW, Jang TS, Kim JW, Kim YD, et al. Dependence of magnetic, phase-transformation and microstructural characteristics on the Cu content of Nd-Fe-B sintered magnet. *Acta Mater*. 2014;66:12.
31. Kwon HW, Lee JG, Yu JH. Origin of radical coercivity reduction in fine Nd-Fe-B-type hydrogenation, disproportionation, desorption, recombination particles and its recovery. *J Appl Phys*. 2014;115(17):30.
32. Corfield MR, Harris IR, Williams AJ. Influence of oxygen content on grain growth in Pr-Fe-B/Nd-Fe-B sintered magnets. *J Alloys Compd*. 2008;463(1–2):180.
33. McGuiness PJ, Short C, Wilson AF, Harris IR. The production and characterization of bonded, hot-pressed and die-upset HDDR magnets. *J Alloys Compd*. 1992;184(2):243.
34. Müller KH, Grünberger W, Hinz D, Gebel B, Eckert D, Handstein A. Hot deformed HDDR Nd-Fe-B permanent magnets. *Mater Lett*. 1998;34(1–2):50.
35. Takagi K, Akada M, Soda R, Ozaki K. Preparation of Nd-Fe-B sintered magnets from HDDR-processed powder. *J Magn Magn Mater*. 2015;393:461.
36. Gopalan R, Sepehri-Amin H, Suresh K, Ohkubo T, Hono K, Nishiuchi T, et al. Anisotropic Nd–Fe–B nanocrystalline magnets processed by spark plasma sintering and in situ hot pressing of hydrogenation–decomposition–desorption–recombination powder. *Scr Mater*. 2009;61(10):978.
37. Suresh K, Ohkubo T, Takahashi YK, Oh-ishi K, Gopalan R, Hono K, et al. Consolidation of hydrogenation-disproportionation-desorption-recombination processed Nd-Fe-B magnets by spark plasma sintering. *J Magn Magn Mater*. 2009;321(22):3681.
38. Ikram A, Mehmood MF, Podlogar M, Eldosouky A, Sheridan RS, Awais M, et al. The sintering mechanism of fully dense and highly coercive Nd-Fe-B magnets from the recycled HDDR powders reprocessed by spark plasma sintering. *J Alloys Compd*. 2019;774:1195.
39. Seelam UMR, Ohkubo T, Abe T, Hirosawa S, Hono K. Faceted shell structure in grain boundary diffusion-processed sintered Nd–Fe–B magnets. *J Alloys Compd*. 2014;617:884.
40. Li WF, Ohkubo T, Hono K, Nishiuchi T, Hirosawa S. The role of grain boundaries in the coercivity of hydrogenation disproportionation desorption recombination processed Nd-Fe-B powders. *J Appl Phys*. 2009;105(7):07A706.
41. Li WF, Ohkubo T, Hono K. Effect of post-sinter annealing on the coercivity and microstructure of Nd–Fe–B permanent magnets. *Acta Mater*. 2009;57(5):1337.
42. Vial F, Joly F, Nevalainen E, Sagawa M, Hiraga K, Park KT. Improvement of coercivity of sintered NdFeB permanent magnets by heat treatment. *J Magn Magn Mater*. 2002;242–245:1329.
43. Güth K, Lyubina J, Gebel B, Schultz L, Gutfleisch O. Ultra-fine grained Nd-Fe-B by high pressure reactive milling and desorption. *J Magn Magn Mater*. 2012;324(18):2731.

44. Sheridan RS, Harris IR, Walton A. The development of microstructure during hydrogenation–disproportionation–desorption–recombination treatment of sintered neodymium-iron-boron-type magnets. *J Magn Magn Mater*. 2016;401:455.
45. Pal SK, Güth K, Woodcock TG, Schultz L, Gutfleisch O. Properties of isolated single crystalline and textured polycrystalline nano/sub-micrometre $Nd_2Fe_{14}B$ particles obtained from milling of HDDR powder. *J Phys D Appl Phys*. 2013;46(37):375004.
46. Wehrenberg C, Daniil M, Willard M, Zande B, Sankar S, Thadhani N. Nanoscale anisotropic Nd-Fe-B particles with high coercivity prepared by attrition milling. *Appl Phys Lett*. 2013;102(22):22311.
47. Gang S, Lianxi H, Erde W. Preparation, microstructure, and magnetic properties of a nanocrystalline Nd12Fe82B6 alloy by HDDR combined with mechanical milling. *J Magn Magn Mater*. 2006;301(2):319.
48. Morimoto K, Katayama N, Akamine H, Itakura M. Coercivity enhancement of anisotropic Dy-free Nd–Fe–B powders by conventional HDDR process. *J Magn Magn Mater*. 2012;324:3723.
49. Sepehri-Amin H, Ohkubo T, Nishiuchi T, Hirosawac S, Hono K. Coercivity enhancement of hydrogenation–disproportionation–desorption–recombination processed Nd–Fe–B powders by the diffusion of Nd–Cu eutectic alloys. *Scr Mater*. 2010;63:1124.
50. Szymański M, Michalski B, Jezierska E, Leonowicz M, Miazga Z. Hydrogen disproportionation phase diagram and magnetic properties for Nd15Fe79B6 alloy. *J Rare Earths*. 2016;34(8):843.
51. Yin XW, Liu M, Wan BC, Zhang Y, Liu WQ, Wu YF, et al. Recycled Nd-Fe-B sintered magnets prepared from sludges by calcium reduction-diffusion process. *J Rare Earths*. 2018;36(12):1284.